Earth, Planets and Space

FULL PAPER Open Access

Chemical heat derived from rocket-borne WADIS-2 experiment

Mykhaylo Grygalashvyly[1*], Boris Strelnikov[1], Irina Strelnikova[1], Markus Rapp[2], Franz-Josef Lübken[1], Corinna Schütt[1], Claudia Stephan[1], Martin Eberhart[3], Stefan Löhle[3] and Stefanos Fasoulas[3]

Abstract

Chemical heating rates were derived from three of the most significant reactions based on the analysis of common volume rocket-borne measurements of temperature, atomic oxygen densities, and neutral air densities. This is one of the first instances of the retrieval of nighttime chemical heat through the utilization of non-emissive observations of atomic oxygen concentrations, obtained through in situ measurements, performed at the Andøya Space Center (69°N, 16°E) at 01:44:00 UTC on 5 March 2015. Furthermore, we determine the heating efficiency for one of the most significant reactions of atomic hydrogen with ozone and illustrate the methodology for such calculations based on known atomic oxygen and temperature. Subsequently, using ozone values obtained from satellite observations, we retrieved odd-hydrogens and total chemical heat. Finally, we compared the retrieved chemical heat with the heat from turbulent energy dissipation. Our findings reveal that the vertically averaged chemical heat is greater than the heat from turbulent energy dissipation throughout the entire mesopause region during nocturnal conditions. The heating rates of turbulent energy dissipation may exceed the chemical heating rates only in narrow peaks, several hundred meters wide.

Keywords Mesopause, Mesosphere–low thermosphere (MLT), Chemical heating rates, Turbulent energy dissipation

*Correspondence:
Mykhaylo Grygalashvyly
gryga@iap-kborn.de
Full list of author information is available at the end of the article

Graphical Abstract

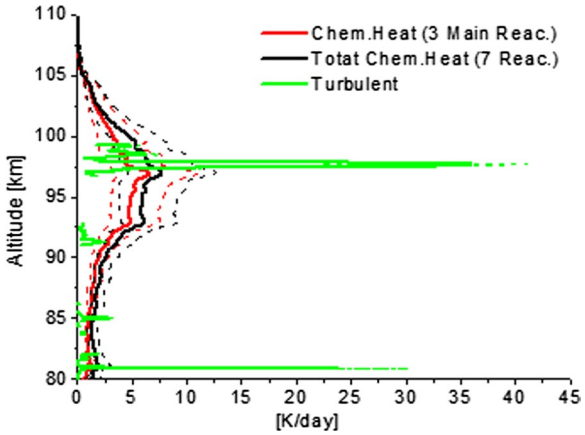

1 Introduction

In the mesopause, space meets the atmosphere, therefore, the energy balance of this region is very complex, as some of the energy comes from above, some from below and some is generated internally. However, the information about energy balance is fundamental to understand the processes occurring in this region. The energy balance is linked to the dynamics and turbulence of this region, which affect the mixing of minor chemical constituents that participate in radiative processes, leading to the organization of complex nonlinear feedbacks between the dynamical, chemical, and radiative subsystems and determining the interaction between the upper and middle atmosphere (e.g., Ward and Fomichev 1993, 1996). Nevertheless, there are still many open questions related to the energy budget in the mesopause region. One of the essential sources of energy in the mesopause is chemical heat released from exothermic reactions.

Kellogg (1961) was one of the first to state that the chemical heat due to exothermic reactions is the important source of energy in the upper mesosphere–lower thermosphere region. Ten years after, the chemical heating rates (CHR) have been investigated by one-dimensional models (Crutzen 1971; Hunt 1972). Following them, the importance of exothermic chemical reactions in the middle atmosphere budget has been noted by many researchers, and have been studied based on observations and modeling (e.g., Garcia and Solomon 1983; Brasseur and Offermann 1986; Mlynczak and Solomon 1991, 1993; Meriwether and Mlynczak 1995). Mlynczak and Solomon (1991, 1993) used distributions of minor chemical constituents from two-dimensional model (Garcia and Solomon 1983, 1985) for the investigations of the CHR and evaluation of the heating efficiency. They found that in mesopause region the effect of total chemical heat (due to main exothermic chemical reactions) may exceed the sum of direct absorption of solar radiation by ozone and molecular oxygen. Results obtained by Meriwether and Mlynczak (1995) to mean that the chemical heat may contribute to the formation of the mesosphere inversion layer (MIL), which was firstly found by Schmidlin (1976) and later on investigated by other authors (e.g., Hauchecorne et al. 1987; She et al. 1993; Ramesh et al. 2013, 2014; and references therein). Nevertheless, Szewczyk et al. (2013) showed that the heat of dissipation of turbulent energy, or other words turbulent heating rates (THR), would be sufficient to form such a layer.

The seasonal, diurnal and latitudinal variations of the minor chemical constituents concentrations lead to variations of the CHR. Thus, three-dimensional modeling is therefore desirable to obtain solid results. The three-dimensional calculations of the CHR were published by Sonnemann et al. (1997, 1998). Following Mlynczak and Solomon (1991) they confirmed that, among all exothermic chemical reactions, three of them, O+O+M, $O+O_2+M$, and $H+O_3$, are the major reactions for chemical heat production.

Riese et al. (1994a, b) have noted that the dynamical effects may essentially influence atomic oxygen concentrations (which have a long enough photochemical lifetime to be transported in mesopause) and consequently CHR. The impact of the diurnal tides on CHR was studied by 3D modeling (Smith et al. 2003). Based on one-dimensional models, the effect of gravity waves (GWs) on CHR has been investigated in a number of works (Hickey and Walterscheid 1994; Xu et al. 2000; Hickey

et al. 2003). While Hickey and Walterscheid (1994) and Xu et al. (2000) found a decrease in CHR, the calculations of Hickey et al. (2003) showed a positive effect. The latter have argued that this is due to the presence of time dependence and non-linear chemistry in their calculations. The effect of realistic (not parameterized) GWs on the CHR due to wave mixing of minor chemical constituents based on 3D calculations with nonlinear chemistry, among other problems, was investigated in the works by Grygalashvyly et al. (2011, 2012). They found that the effect in mesopause could be positive as well as negative depending on altitude (positive below ~85 to 90 km and negative above), latitudes, and seasons.

Besides modeling CHR was investigated based on satellite observations. One of the first who used satellite observations of solar mesosphere explorer (SME) to calculate CHR rates were Riese et al. (1994a, 1994b). They found larger values (approx. two times) than those predicted by modeling (e.g., Mlynczak and Solomon 1993). Based on data obtained by the sounding of atmosphere by broadband radiometry (SABER) instrument onboard of thermosphere ionosphere mesosphere energetics and dynamics (TIMED) satellite (Mlynczak 1997; Mlynczak et al. 2013a; Esplin et al. 2023), Ramesh et al. (2013) concluded that the chemical heat is a primary factor for mesospheric inversion layer formation in some cases, nevertheless, the dynamical reasons may dominate over the chemical heat too. The authors also found that in the region 80–90 km, the reaction of ozone with atomic hydrogen dominates over other exothermic chemical reactions. Later on, the tripled MIL has been found in light detection and ranging (LIDAR) temperature observations over Gadanki (13.5°N; 79°E) in India (Ramesh et al. 2014). An analysis using the SABER data revealed that the lowest peak at 70 km occurs because of planetary waves dissipation, the middle one at 80 km is the result of GWs breaking and subsequent turbulent dissipation, whereas the peak above 90 km is formed because of chemical heat, mainly from the reaction of atomic oxygen recombination, with values of energy release up to ~45 K per day. Ramesh et al. (2015) by calculations based on SABER data found very large total CHR at low latitudes (10°N–15°N) with values of ~15 to 20 K/day below 95 km and up to ~100 K/day above 95 km. The authors found that the primary reaction in the region under investigation is the reaction of atomic oxygen recombination. The reaction of ozone with atomic hydrogen essentially contributes to total CHR as the secondary source below 95 km. Also, the authors found that the 11-year variation in solar activity has an impact on CHR. Later it was shown that the nighttime values of total CHR are larger than those of daytime at low latitudes and CHR has strong seasonal variability, which is different for night and day (Ramesh et al. 2017). Partially, among other topics, CHR has been touched on in a number of works, which are based on SABER observations, for example, to derive energetic constraints on atomic oxygen concentrations for global annual mean values (Mlynczak et al. 2007, 2013b, 2013c, 2018).

Another important source of the heat budget of mesopause is turbulence (e.g., von Zahn et al. 1990). A very wide range of values of THR near mesopause (from several up to more than 40 K/day) can be found in the literature (e.g., Justus 1967; Chandra 1980; Gordiets et al. 1982; Hocking 1990). The most precise and detailed measurements of the turbulence field in the MLT are made using ionization gauges onboard sounding rockets, as it was shown by Strelnikov et al. (2023). Using this technique, it was found in a series of rocket-borne observations that at high latitudes in mesopause the THR have strong seasonality with values ~10 to 20 K/day in summer and ~1–2 K/day in winter (Lübken et al. 1993, 2002; Lübken 1997).

These very diverse values lead to very different conclusions on the relative importance of exothermic CHR and THR in the energetic balance of mesopause. Up to now,

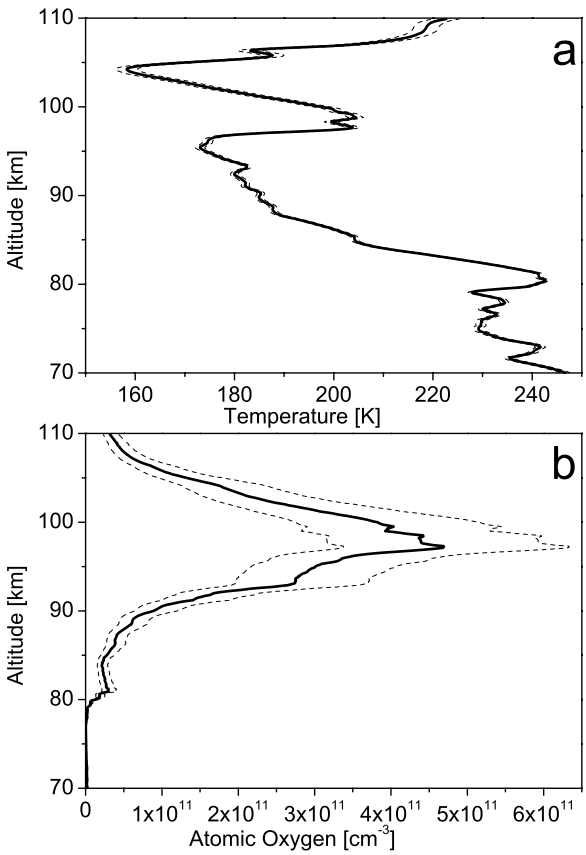

Fig. 1 Measurements of **a** temperature (CONE), **b** atomic oxygen concentration (FIPEX). The *dashed lines* represent an uncertainty

there is no unambiguous opinion of what prevails in the mesopause—CHR or THR.

In this paper, for the first time, based on common volume measurements of temperature, concentration of air and atomic oxygen from the wave propagation and dissipation in the middle atmosphere (WADIS-2) sounding rocket campaign, we address this question. The rocket experiment and obtained data relevant for this work are described in the next section. The calculations and some theoretical aspects are discussed in section three. The results and their discussion are given in section four. The conclusions are summarized in the last section.

2 Rocket-borne experiment

The WADIS experiment aimed to study how waves move through the middle atmosphere, how that affects the energy budget, and how it affects the concentration of trace constituents (Strelnikov et al. 2019). The great thing about this experiment is that we can measure the concentrations of atomic oxygen, temperature and volume emission of atmospheric bands simultaneously. The WADIS-2 sounding rocket was launched at the Andøya Space Center (69°N, 16°E) at 01:44:00 UTC on 5 March 2015 [see Strelnikov et al. (2017, 2019), for more details]. Two main data providers for this study are the combined sensor for neutrals and electrons (CONE) and flux probe experiment (FIPEX) instruments.

The CONE instrument, made by IAP (Leibniz Institute of Atmospheric Physics at Rostock University), is a combination of an ionization gauge for neutral density measurements and of a fixed biased Langmuir probe for electron density measurements (Strelnikov et al. 2013). In this work, only the neutral density measurements by the CONE are used. Making use of laboratory calibrations allows to derive absolute number density of neutral air in the altitude range 70–110 km. The derived density profile is further integrated, assuming hydrostatic equilibrium, to yield a temperature altitude-profile (Strelnikov et al. 2013, and the references therein).

The FIPEX instrument, developed by the Institute of Space Systems at the University of Stuttgart (IRS), measures the concentration of atomic oxygen along the rocket flight trajectory. It uses a solid electrolyte sensor that is sensitive to atomic oxygen. The current, which

Table 1 List of reactions with corresponding reaction rates r_{1-12} [for three-body reactions (cm^6 $molecule^{-2}$ s^{-1}) and for two-body reactions (cm^3 $molecule^{-1}$ s^{-1})], branching ratios $f_{v=9,\ldots,5}$, quenching coefficients $Q_{vv'}$, q_v, $p_{vv'}$ (cm^3 $molecule^{-1}$ s^{-1}), spontaneous emission coefficients $A_{vv'}$ (s^{-1}) and energy releases ϵ_{1-7} (kcal/mole) of exothermic chemical reactions used in the paper

	Reaction	Coefficient	References
1	$O + O + M \rightarrow O_2 + M$	$r_1 = 4.7 \times 10^{-33}(300/T)^2$ $\epsilon_1 = 119.40$	Campbell and Gray (1973)
2	$O + O_2 + M \rightarrow O_3 + M$	$r_2 = 6.1 \times 10^{-34}(298/T)^{2.4}$ $\epsilon_2 = 25.47$	Burkholder et al. (2020)
3	$O + O_3 \rightarrow 2O_2$	$r_3 = 8 \times 10^{-12}\exp\left(\frac{-2060}{T}\right)$ $\epsilon_3 = 93.65$	Burkholder et al. (2020)
4	$H + O_3 \overset{f_v r_4}{\rightarrow} OH_{v=5,\ldots,9} + O_2$	$r_4 = 1.4 \times 10^{-10}\exp\left(\frac{-470}{T}\right)$ $f_{v=9,\ldots,5} = 0.47, 0.34, 0.15, 0.03, 0.01$ $\epsilon_4 = 76.9$	Burkholder et al. (2020), Adler-Golden (1997)
5	$O + OH \rightarrow O_2 + H$	$r_5 = 1.8 \times 10^{-11}\exp\left(\frac{180}{T}\right)$ $\epsilon_5 = 16.77$	Burkholder et al. (2020)
6	$O + HO_2 \rightarrow O_2 + OH$	$r_6 = 3 \times 10^{-11}\exp\left(\frac{200}{T}\right)$ $\epsilon_6 = 53.27$	Burkholder et al. (2020)
7	$H + O_2 + M \rightarrow HO_2 + M$	$r_7 = 5.3 \times 10^{-32}(298/T)^{1.8}$ $\epsilon_7 = 49.1$	Burkholder et al. (2020)
8	$H + HO_2 \rightarrow O_2 + H_2$	$r_8 = 6.9 \times 10^{-12}$	Burkholder et al. (2020)
9	$H + HO_2 \rightarrow O + H_2O$	$r_9 = 1.6 \times 10^{-12}$	Burkholder et al. (2020)
10	$H + HO_2 \rightarrow 2OH$	$r_{10} = 7.2 \times 10^{-11}$	Burkholder et al. (2020)
11	$OH + O_3 \rightarrow HO_2 + O_2$	$r_{11} = 1.7 \times \exp\left(\frac{-940}{T}\right)$	Burkholder et al. (2020)
12	$O + OH_{v=1,..,9} \rightarrow O_2 + H$	$r_{12}(v = 9, \ldots, 1)$	Caridade et al. (2013)
13	$OH_v + O_2, N_2, O \rightarrow OH_{v'<v} + O_2, N_2, O$	$Q_{vv'}$, q_v, $p_{vv'}$, see text	Adler-Golden (1997), Makhlouf et al. (1995), Caridade et al. (2013)
14	$OH_v \rightarrow OH_{v'<v} + hv$	$A_{vv'}$	Xu et al. (2012)

v is vibrational number

is measured between the anode and cathode with a low voltage applied between the electrodes, is a function of the oxygen concentration. The fast sensor response allows to resolve spatial scales on the order of tens of meters. The reader can find more details about this instrument and the calibration techniques in the works of Eberhart et al. (2015, 2019). For a full overview of all the instruments and the rocket flight, see Strelnikov et al. (2019).

Figure 1 shows the data from the rocket campaign that we used in our calculations. It includes the temperature from the CONE instrument (a) and atomic oxygen concentration measured by FIPEX (b). One can find more details about how WADIS-2 compares to other measurements and modeling in a number of papers (e.g., Eberhart et al. 2019; Strelnikov et al. 2017, 2018).

The measured profiles of neutral air density can be found in Strelnikov et al. (2019) and Grygalashvyly et al. (2019). Since the composition of the neutral air at altitudes 70 to 100 km to a good approximation can be considered constant, one can use the CONE measurements and partitioning based on the reference atmosphere model NRLMSISE-00 (Picone et al. 2002), to derive the molecular oxygen and molecular nitrogen concentrations.

3 Approaches and calculations

In Table 1 we have collected all reactions with corresponding reaction rates r_{1-12}, branching ratios $f_{v=9,\ldots,5}$, quenching coefficients $Q_{vv'}, q_v, p_{vv'}$, spontaneous emission coefficients $A_{vv'}$ and energy releases ϵ_{1-7} of exothermic chemical reactions used in the paper, as well corresponding references. M is concentration of surrounding air, and O, O_3, H, OH, HO_2, O_2, N_2 are the chemical substances. The subscript v denotes vibrational number of the vibrationally excited hydroxyl $OH_{v=1,..,9}$.

Note, that in our work we consider the chemical heat only from exothermic chemical reactions (1–7 in Table 1). The processes of radiative excitation followed by relaxation and thermalization are omitted.

We will use the ozone balance equation assuming that ozone is in photochemical equilibrium for nighttime conditions:

$$r_2\mathrm{M}\cdot\mathrm{O}\cdot\mathrm{O}_2 = r_4\mathrm{H}\cdot\mathrm{O}_3 + r_3\mathrm{O}\cdot\mathrm{O}_3. \tag{1}$$

Hereafter, in equations, the symbols of chemical substances denote corresponding concentrations. Following Smith et al. (2008), we consider last term as non-effective loss, which constitutes ~5% of total ozone losses at nighttime conditions, hence

$$r_2\mathrm{M}\cdot\mathrm{O}\cdot\mathrm{O}_2 = r_4\mathrm{H}\cdot\mathrm{O}_3. \tag{2}$$

In order to prove the assumption about ozone photochemical equilibrium we utilize criterion, which was derived and proved by Kulikov et al. (2018), and applied in number of papers (Fytterer et al. 2019; Zhu and Kaufmann 2019; Kulikov et al. 2019, 2021).

Following Kulikov et al. (2018):

$$\frac{2r_7r_2(\mathrm{M}\cdot\mathrm{O}_2)^2}{r_4^2\cdot\mathrm{H}\cdot\mathrm{O}_3}\left(1-\frac{r_8+r_9}{r_6}\right)\le 0.1. \tag{3}$$

This criterion is necessary and sufficient (Kulikov et al. 2023). For utilizing it in our work, we rewrite it in terms of atomic oxygen, substituting in original criterion the term $r_4\mathrm{H}\cdot\mathrm{O}_3$ in denominator from ozone balance Eq. (2):

$$\frac{2r_7M\cdot\mathrm{O}_2}{r_4\cdot\mathrm{O}}\left(1-\frac{r_8+r_9}{r_6}\right)\le 0.1. \tag{4}$$

Figure 2 depicts values of left-hand side (LHS) of Eq. (4). One can see that LHS of Eq. (4) becomes smaller than 0.1 above ~78 km, and taking into account uncertainties (dashed line) above 80 km. As with other figures, the dashed lines show the uncertainties, which represent the error propagation. These have been calculated according to Bevington and Robinson (2003). Hence, the ozone is in equilibrium above this altitude. Further calculations will be carried out above 80 km.

It was marked in number of works that the chemical heat in mesopause region at night is produced mainly by three exothermic reactions: O+O+M, O+O_2+M, and H+O_3 (Mlynczak and Solomon 1991; Sonnemann et al. 1997, 1998; Smith et al. 2003). Knowing only atomic oxygen, we may calculate energy release for all of them. Main exothermic chemical energy release (E_{main}) is given by following equation:

$$E_{\mathrm{main}} = \epsilon_1 r_1\mathrm{M}\cdot\mathrm{O}^2 + \epsilon_2 r_2\mathrm{M}\cdot\mathrm{O}\cdot\mathrm{O}_2 + \varepsilon\cdot\epsilon_4 r_4\mathrm{H}\cdot\mathrm{O}_3, \tag{5}$$

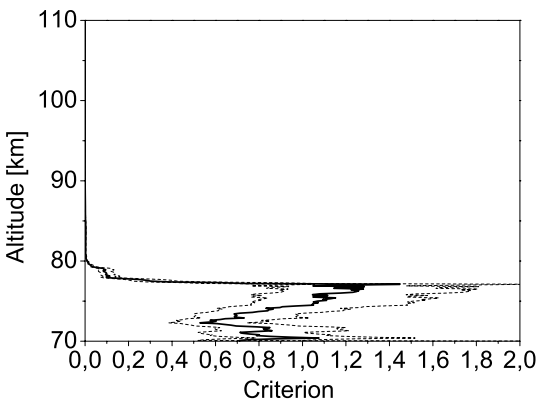

Fig. 2 Calculated values of ozone chemical equilibrium criterion (LHS of Eq. 4). The *dashed lines* represent an uncertainty

where ε is the efficiency for reaction of atomic hydrogen with ozone.

By efficiency, following McDade and Llewellyn (1991, 1993), Mlynczak and Solomon (1993), Smith et al. (2015), we mean the relative (to the total) part of exothermic chemical reaction energy release that goes to thermalization. The efficiencies for the first two reactions, following Mlynczak and Solomon (1993), are assumed to be one. We conduct calculations only in the region where ozone in photochemical equilibrium. Substituting Eq. (2) into Eq. (5), we obtain:

$$E_{\text{main}} = \epsilon_1 r_1 \mathrm{M}\cdot\mathrm{O}^2 + (\epsilon_2 + \varepsilon\cdot\epsilon_4) r_2 \mathrm{M}\cdot\mathrm{O}\cdot\mathrm{O}_2. \tag{6}$$

In order to calculate the efficiency ε, at the beginning, we calculate distributions of $\mathrm{OH}_{v=1-9}$. Assuming photochemical equilibrium for excited hydroxyl, its concentration can be calculated as the ratio of productions to the losses (e.g., Grygalashvyly et al. 2021):

$$\mathrm{OH}_v = \frac{\left(\begin{array}{c} f_v r_4 H\cdot\mathrm{O}_3 + \sum_{v'=v+1}^{9} p_{v'v}\mathrm{OH}_{v'}O + q_{v+1}\mathrm{OH}_{v+1}\mathrm{N}_2 + \\ + \sum_{v'=v+1}^{9} Q_{v'v}\mathrm{OH}_{v'}\mathrm{O}_2 + \sum_{v'=v+1}^{9} A_{v'v}\mathrm{OH}_{v'} \end{array}\right)}{r_{12}(v)\mathrm{O} + \sum_{v''=0}^{v-1} p_{vv''}\mathrm{O} + q_v\mathrm{N}_2 + \sum_{v''=0}^{v-1} Q_{vv''}\mathrm{O}_2 + \sum_{v''=0}^{v-1} A_{vv''}}, \left(\begin{array}{c} v < v' \\ v'' < v \end{array}\right). \tag{7}$$

Here, v is the vibrational number, f_v are the branching ratios for the reaction of ozone with atomic hydrogen (Table 1 in Adler-Golden 1997); $r_{12}(v)$ are the rates for the reaction of atomic oxygen with excited hydroxyl (Table 1 in Caridade et al. 2013); p, q, Q are the rates for quenching by atomic oxygen (Table 1 in Caridade et al. 2013), by molecular nitrogen (Table 1 in Makhlouf et al. 1995), and by molecular oxygen (Table 3 in Adler-Golden 1997), respectively. Further, $A_{v'v}$ are the Einstein coefficients for spontaneous emission (Xu et al. 2012). In contrast to work Grygalashvyly et al. (2021), in our current paper we apply the temperature dependence of the reaction rates of atomic oxygen with excited hydroxyl (r_{12}) and quenching coefficients for atomic oxygen (p) by taking values for 110, 160, 210, 255 K (Table 1 in Caridade et al. 2013) and linearly interpolating between these points, as this approach is more refined. Theoretically derived quenching ratios for molecular oxygen are assumed to be overestimated [see discussion in Fytterer et al. (2019), Sect. 2.3, page 1839]; hence, following Xu et al. (2012), we multiply it by factor $\alpha = 0.723$. Besides quenching ratios and spontaneous emission coefficients for excited hydroxyl, which one can find in corresponding papers (Adler-Golden 1997; Caridade et al. 2013; Xu et al. 2012), all of the other used reactions are collected in Table 1 with corresponding reaction rates, branching ratios, and references. Recently, new mechanism of $\mathrm{O}(^1\mathrm{D})$ formation from excited hydroxyl was proposed (Sharma et al. 2015; Kalogerakis et al. 2016; Kalogerakis 2019). We omit this mechanism in our consideration, because currently it has hypothetical character and it needs laboratory and observational confirmations.

We utilize that the ozone is in chemical equilibrium above 80 km at nighttime conditions (Fig. 2). Substituting Eq. (2) into the excited hydroxyl balance equation (first term in the numerator of Eq. 7), we obtain an expressions for OH_v in terms of atomic oxygen and temperature:

$$\mathrm{OH}_v = \frac{\left(\begin{array}{c} f_v r_2 M\cdot O\cdot\mathrm{O}_2 + \sum_{v'=v+1}^{9} p_{v'v}\mathrm{OH}_{v'}O + q_{v+1}\mathrm{OH}_{v+1}\mathrm{N}_2 + \\ + \sum_{v'=v+1}^{9} Q_{v'v}\mathrm{OH}_{v'}\mathrm{O}_2 + \sum_{v'=v+1}^{9} A_{v'v}\mathrm{OH}_{v'} \end{array}\right)}{r_{12}(v)\mathrm{O} + \sum_{v''=0}^{v-1} p_{vv''}\mathrm{O} + q_v\mathrm{N}_2 + \sum_{v''=0}^{v-1} Q_{vv''}\mathrm{O}_2 + \sum_{v''=0}^{v-1} A_{vv''}}, \left(\begin{array}{c} v < v' \\ v'' < v \end{array}\right). \tag{8}$$

At the next step, we calculate efficiency (e.g., Smith et al. 2015):

$$\varepsilon = 1 - \frac{\sum_{v=1}^{v=9}\mathrm{OH}_v\left(\sum_{v''=0}^{v-1} A_{vv''}\theta_{vv''}\right)}{\epsilon_4 r_2 \mathrm{M}\cdot\mathrm{O}\cdot\mathrm{O}_2}, \left(v'' < v\right), \tag{9}$$

where $\theta_{vv''}$ are the energies of photons for corresponding transitions (see Khomich et al. 2008; Table 2.1). Then, we calculated CHR with Eq. (6). Hence, the main part of CHR is based on self-consistent calculations because it takes into account the data obtained only from our common volume observations for all measured parameters.

Nevertheless, it is desirable to assess the total CHR. In order to calculate the rest of CHR, we use ozone from SABER observations. In this case we lose self-consistency but acquire possibility to calculate total CHR, including additionally four secondary reactions ($\mathrm{O}+\mathrm{O}_3$, $\mathrm{OH}+\mathrm{O}$, $\mathrm{HO}_2+\mathrm{O}$, and $\mathrm{H}+\mathrm{O}_2+\mathrm{M}$). For these purposes, we use chemical equilibrium of ground state hydroxyl and hydroperoxy radicals (here we denote their concentrations as OH and HO_2, respectively) in mesopause region at nighttime conditions, and write their balance equations (e.gBrasseur and Offermann 1986; Brasseur and Solomon 2005):

$$\begin{aligned} & r_4\mathrm{H}\cdot\mathrm{O}_3 + r_6\mathrm{O}\cdot\mathrm{HO}_2 + 2r_{10}\mathrm{H}\cdot\mathrm{HO}_2 \\ & \quad = r_5\mathrm{O}\cdot\mathrm{OH} + r_{11}\mathrm{O}_3\cdot\mathrm{OH}, \end{aligned} \tag{10}$$

$$r_6\mathrm{O}\cdot\mathrm{HO}_2+(r_8+r_9+r_{10})\mathrm{H}\cdot\mathrm{HO}_2 = r_7\mathrm{H}\cdot\mathrm{O}_2\cdot\mathrm{M}+r_{11}\mathrm{O}_3\cdot\mathrm{OH}. \quad (11)$$

Note, it was shown recently that OH and HO_2 are in photochemical equilibrium in March at high latitudes above 80 km (Kulikov et al. 2024).

Equations (2), (10), and (11) represent linear system with three unknown variables: atomic hydrogen, hydroxyl and hydroperoxy radicals. From the system we obtain:

$$\mathrm{H}=\frac{r_2\mathrm{O}_2\cdot\mathrm{M}\cdot\mathrm{O}}{r_4\mathrm{O}_3}, \quad (12)$$

$$\mathrm{HO}_2=\frac{r_7\mathrm{H}\cdot\mathrm{O}_2\cdot\mathrm{M}+r_{11}\mathrm{O}_3\cdot\mathrm{OH}}{r_6\mathrm{O}+(r_8+r_9+r_{10})\mathrm{H}}, \quad (13)$$

$$\mathrm{OH}=\frac{r_4\mathrm{H}\cdot\mathrm{O}_3+r_6\mathrm{O}\cdot\mathrm{HO}_2+2r_{10}\mathrm{H}\cdot\mathrm{HO}_2}{r_5\mathrm{O}+r_{11}\mathrm{O}_3}. \quad (14)$$

Knowing all odd-oxygen $(\mathrm{O},\mathrm{O}_3)$ and odd-hydrogen $(\mathrm{H},\ \mathrm{OH},\mathrm{HO}_2)$ concentrations, we calculate total CHR:

$$E_{\text{total}}=E_{\text{main}}+\epsilon_3 r_3\mathrm{O}\cdot\mathrm{O}_3+\epsilon_5 r_5\mathrm{O}\cdot\mathrm{OH}+\epsilon_6 r_6\mathrm{O}\cdot\mathrm{HO}_2+\epsilon_7 r_7\mathrm{H}\cdot\mathrm{O}_2\cdot\mathrm{M}. \quad (15)$$

Finally, we derive THR, ε from neutral density fluctuation (Lübken et al. 1993, 2002; Lübken 1997; Strelnikov et al. 2013), which is further converted into the THR as $\mathrm{d}T/\mathrm{d}t=\varepsilon/c_\mathrm{p}$, where $c_\mathrm{p}=1004$ J kg^{-1} K^{-1} is heat capacity at constant pressure. This method has been validated on direct numerical simulations by Strelnikov et al. (2023). The detailed data description can be found in Strelnikov et al. (2019), as well derivation of the profile. Here, we briefly summarize the most important steps. Fluctuations of neutral air density are measured by ionization gauge CONE. A wavelet transform is applied to these fluctuations. The spectral model of Tatarskii (1971) is subsequently fitted to global wavelet spectra, which are averaged over 100 m altitude range. The spectral models utilize kinematic viscosity, which is derived from the density and temperature as recommended by the U.S. Standard Atmosphere (Minzner 1977), i.e., using the Sutherland's law (Sutherland 1893). The ionization gauge CONE owing to laboratory calibrations measures the absolute density. The measured density altitude-profile is integrated assuming hydrostatic equilibrium, yielding the temperature profile. That is, the turbulence energy dissipation rates are entirely derived from measurements. In this work we only use turbulence analysis results, derived based on the spectral model of Tatarskii (1971), since they reveal smaller uncertainty as shown by Strelnikov et al. (2023). Then we compare the CHR and THR. In the next section, we show and discuss the results of our calculations.

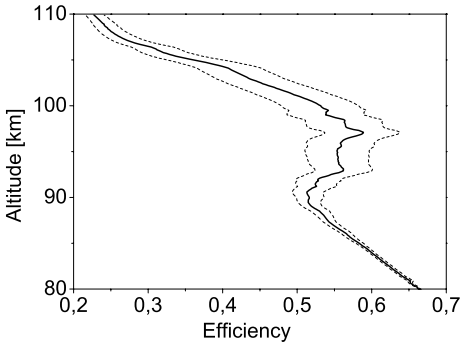

Fig. 3 The efficiency of the reaction four calculated from Eqs. (8) and (9). The *dashed lines* represent an uncertainty

4 Results and discussion

Figure 3 shows efficiency of the reaction of ozone with atomic hydrogen calculated according to Eq. (9). This value shows which part of energy is thermalized (the remainder goes to spontaneous emission). This value decreases with altitude as the concentration of the main quencher, molecular oxygen, decreases, hence, the thermalization processes. Nevertheless, there is a peak at an altitude of 97 km, where the thermalization processes increase, exactly coinciding with the peak of atomic oxygen (Fig. 1b), which is the second most important quencher for OH*. The efficiency varies between ~0.65 and 0.5 in the region 80–100 km, where this reaction is important. McDade and Llewellyn (1991) found that the efficiency for this reaction at 90 km amounts to 0.65–0.81, depending on the scheme of OH* relaxation and spontaneous emission parameters. Mlynczak and Solomon (1993) assessed these values with four different models of OH* relaxation, found the values 0.3–1, depending on model and altitude, and recommend for utilization 0.6 through the entire mesopause. Based on three different sets of spontaneous emission coefficients McDade and Llewellyn (1993) found three efficiency profiles with range ~0.85 to 0.95 at 80 km down to 0.35–0.5 at 100 km and recommended value 0.75 near the mesopause at night. Note, that they obtained smooth profiles without peaks because atomic oxygen quenching was omitted in their scheme (Fig. 3 in McDade and Llewellyn 1993). Later on, based on Whole Atmosphere Community Climate Model accompanied by model of vibrationally excited hydroxyl, Smith et al. (2015) proposed parametrization for the efficiency as a fit-function of pressure, temperature and atomic oxygen concentration in the mesopause region. The globally averaged annual mean vertical profile of the efficiency obtained from this

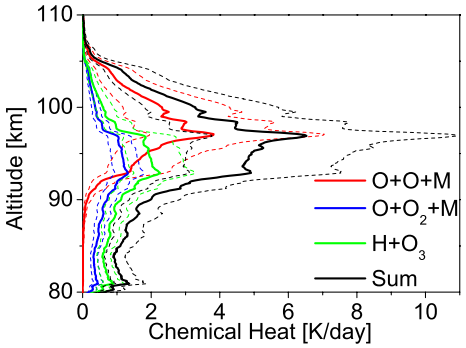

Fig. 4 Main part of CHR from three most important exothermic reactions from self-consistent common volume WADIS-2 experiment: reaction 1 (*red line*), reaction 2 (*blue line*), reaction 4 (*green line*), and their sum (*black line*). The *dashed lines* represent corresponding uncertainties

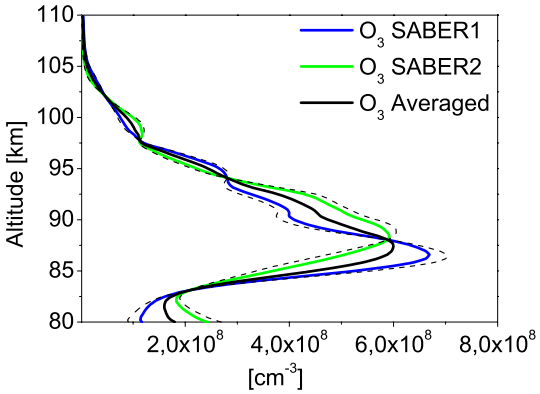

Fig. 5 Ozone from SABER observations (orbit number 71729 event number 19 and 20, *blue* and *green lines*, respectively), their averaged (*black line*) and standard deviations (*dashed lines*)

work is very similar with our one. The values amount to ~0.65 at 80 km, ~0.4 at 110 km, with local peak ~0.65 between 90 and 100 km (Fig. 3b in Smith et al. 2015). This peak occurs because the parametrization takes into account atomic oxygen. Smith et al. (2015) conclude that "the efficiency is almost identical during day and night", hence, the way of calculations obtained in our work for nighttime is acceptable (for the first approximation) for the daytime.

Figure 4 depicts the altitude profiles of the main part of CHR from three most important reactions: O+O+M (red line), $O+O_2+M$ (blue line), $H+O_3$ (green line), and their sum (black line). The dominating source of CHR above 95 km is the reaction of atomic oxygen recombination with peak values ~4 K/day at 97 km, whereas below the reaction of ozone with atomic oxygen is the leading one with peak more than 2 K/day at ~92–93 km. The total CHR reach values more than 6 K/day at 97 km.

The local night values are not representative of the global mean and the difference between two local profiles can be large due to dynamics and turbulence. However, below we discuss our results in comparison with previous results obtained for the averaged and local scales to make sure that the order of values and heights are similar and to identify common features. The similar results were obtained for globally averaged diurnal mean CHR based on three-dimensional modeling in Spring (Sonnemann et al. 1997, 1998)—the leading reactions are the reactions of atomic oxygen recombination and ozone with atomic hydrogen above and below ~88–90 km, respectively with values ~2.5 to 3.5 K/day at their peaks. Smith et al. (2003) by means of modeling found that in midnight at the equator the CHR from the reaction R1 is higher than those of R4 above ~97 km with values at the peak 13 K/day at 102 km and 6.5 K/day at 93 km, respectively. Ramesh et al. (2014) retrieved from SABER observations a very strong event for 23 September 2011 over Gadanki (13.5°N, 77.8°E) with CHR from R1 more than 40 K/day at ~95 km, which exceed those of R4 above 93 km. A comparison of absolute values of CHR is not very informative because it strongly depends on the situation with gravity waves and tides, season, latitude, and time of day. Nevertheless, it is possible to distinguish features that are common for all measurements and modeling: (1) there is an altitude above which CHR of R1 is stronger than those of R4; (2) this altitude depends on temperature and atomic oxygen concentrations (trivially seen from equality of the first and last terms in Eq. 6).

In order to assess the CHR from other four reactions and total CHR we adopt ozone from SABER observations (Version 2.07, Level 2A, Orbit Number 71729). We took two ozone profiles observed most closely to Andøya Space Center (69°N, 16°E) in this night at high latitudes (67.28°N, 22.10°E and 71.17°N, 18.8°E, with time of observations 22:05 UTC and 22:06 UTC, respectively), calculate their averaged and standard deviations from averaged. The standard deviations will further be used together with the atomic oxygen to calculate errors, and the mean value to calculate odd-hydrogens.

Figure 5 shows ozone profiles observed at 67.28°N 22.10°E (blue line) and at 71.17°N 18.8°E (green line), with time of observations 22:05 UTC and 22:06 UTC, respectively, their averaged (black solid line), and standard deviations from averaged (dashed lines). Then we calculate odd-hydrogens according Eqs. (12–14).

Figure 6 shows concentrations of atomic hydrogen (a), hydroperoxy radicals (b), and hydroxyl (c) calculated

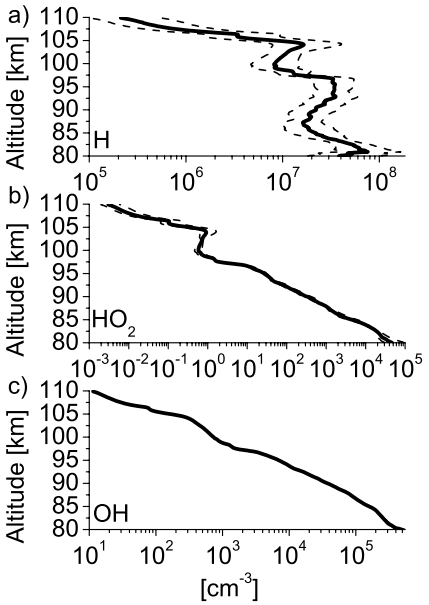

Fig. 6 Calculated by Eqs. (12–14) concentrations of H (**a**), HO_2 (**b**), and OH (**c**). The *dashed lines* represent an uncertainty

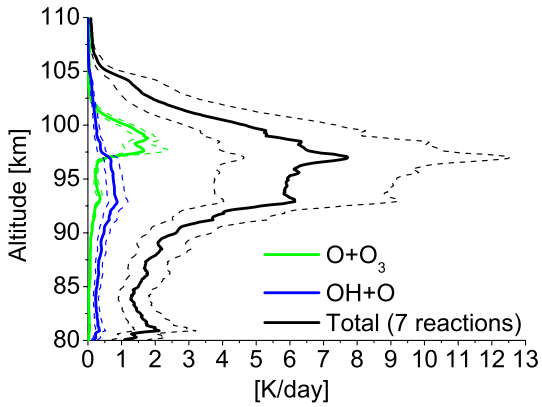

Fig. 7 CHR from secondary exothermic chemical reactions and total CHR from all of seven exothermic chemical reactions. The *dashed lines* represent corresponding uncertainties

from ozone balance equation and equations for odd-hydrogens equilibrium. There are not many observations for OH at the mesopause. Minschwaner et al. (2011) found by Aura Microwave Limb Sounder observations one order larger concentrations of hydroxyl (~10^6 cm^{-3}) at 80 km, but for the daytime conditions, when additional source by dissociation of water vapor exists. Kreyling et al. (2013) by SMILES/ISS (Submillimeter-Wave Limb-Emission Sounder/International Space Station) observed 0.5–3.5 ppbv of nighttime HO_2 near the equator between 80 and 90 km that corresponds to ~10^5–10^6 cm^{-3}. Similar values of HO_2 concentrations (~10^5 cm^{-3}) at 80–85 km declining with altitude were detected by Submillimeter wave Radiometer at Odin satellite in southern winter and several other observations (Baron et al. 2009; Wang et al. 2015; Millàn et al. 2015). As we expected the concentrations of hydroxyl are larger than those of hydroperoxy radicals, and atomic hydrogen is most abundant among other odd-hydrogens in this region.

Figure 7 shows CHR from reaction of ozone with atomic oxygen (green line), hydroxyl with atomic oxygen (blue line), and total CHR (black line) from all seven exothermic chemical reactions (Eq. 15). The profiles for reactions HO_2+O, and H+O_2+M are not shown here, because we found that maximal values for each amounts of ~0.2–0.3 K/day at ~82 km, and they do not exceed 0.1 K/day through the rest of the entire region. Such low values of CHR from these two reactions were also inferred by SABER observations at region 80–100 km in night (Ramesh et al. 2013, 2015, 2017). In region 97–100 km reaction of ozone with atomic oxygen may give CHR ~1.5 K/day, becoming second most important for CHR after the reaction of atomic oxygen recombination. Calculated total CHR has largest values at ~92 to 100 km, with peak up to ~7.5 K/day at 97 km. The resulting local value appears to be quite moderate. Thus, analyzing SABER data, Ramesh et al. (2015) found that CHR can reach values of 100 K/day at altitudes of about 100 km and above, and about 50–60 K/day at altitudes of 90–100 km for monthly mean zonally averaged values. Such averaging procedure mixed the daytime and nighttime values, which could be essentially different. A number of authors note that nocturnal CHR is greater than daytime one (Sonnemann et al. 1997, 1998; Smith et al. 2015). Analysis of SABER observations shows that daytime values of CHR are generally smaller than nocturnal, but may exceed nighttime ones near 100 km and above (Ramesh et al. 2017). The excess of night values over day values, that is typically found on models and confirmed by satellite observations in the 80–110 km region, can be proved analytically for the case, when the daytime downward directed fluxes of atomic oxygen due to turbulent diffusion and/or advection do not exceed the night fluxes, or when there is no large difference in the fluxes for day and night (see Appendix A).

Figure 8 gives the comparison of CHR with THR. The values of THR, which are less than uncertainties are excluded from consideration. THR profile (green line) has been derived in Strelnikov et al. (2019). Blue line shows total CHR profile from SABER (Version 2.07, Level 2B, Orbit Number 71729). In order to obtain profile for comparison we took two CHR profiles observed most closely to our one in this night [(67.28°N 22.10°E) and (71.17°N 18.8°E), with time of observations 22:05 UTC

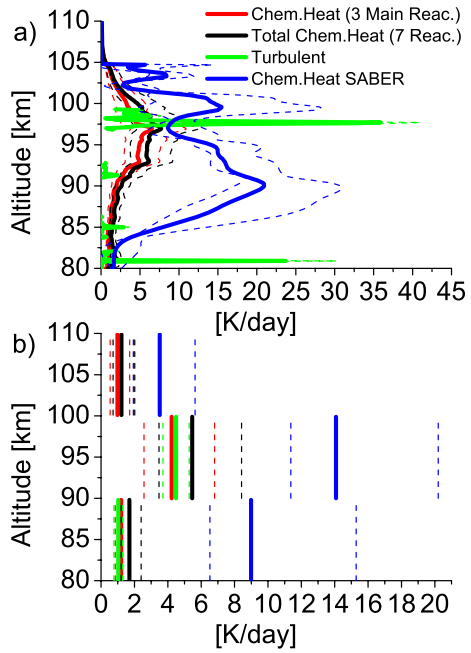

Fig. 8 Comparison of total CHR (*black lines*), main part of CHR (*red line*), THR (*green line*), and total CHR from SABER (*blue line*): **a** local, **b** vertically averaged. The *dashed lines* represent corresponding uncertainties

and 22:06 UTC, respectively], calculate their averaged and standard deviations from averaged.

In Fig. 8a one can see that the CHR from three main reactions (red line) is not so far from the total CHR (black line). Also we can find that the THR (green line) exceeds CHR only in narrow spikes with width several hundred meters, in the rest of the region it does not. It is interesting to note that the peaks of atomic oxygen (and CHR, because it is quadratically proportional to the atomic oxygen concentrations) at 97 km and at 81 km (Fig. 1b) are placed at the peaks of THR. This tells us that turbulence is the essential process of atomic oxygen transport in the mesopause region. The chemical heat according to SABER data has larger values than those obtained by us. This can be explained both by different dynamics at remotely distant points and by "burning out" odd-hydrogens at night (Sonnemann and Grygalashvyly 2020), since our experiment was performed more than three hours later.

Figure 8b shows vertically averaged over 10 km values. The points where the THR are less than error are excluded from the averaging procedure. The THR are comparable with CHR from three main reactions and smaller than total CHR through the entire mesopause. An alternative, to set the THR at excluded points to zero and include them in the average. This would give much lower values for the averages (not shown here).

It was noted that turbulence leads to homogenization of vertical distributions of minor chemical constituents in the mesopause (von Zahn et al. 1990). Atomic oxygen is produced in the lower thermosphere (where it has long photochemical lifetime) during daytime by photo-dissociation and transported down (among other processes by turbulence) in mesopause, where it has chemical losses by recombination (Swenson et al. 2021, and references therein). Mixing ratio of the atomic hydrogen, that is most abundant odd-hydrogen in mesopause region, has positive gradient in there (Mlynczak et al. 2014). Both these constituents are affected by downward vertical transport by turbulence. Increase in turbulence, in turn, leads to acceleration of chemical processes in the vicinity of the mesopause and release of chemical heat. This is one of the possible mechanisms that may help to explain the increase of CHR with increasing turbulence, which we can note in Fig. 8b.

Here was discussed just a case of studies on local scales. Certainly, it is necessary more common volume experiments, which may be able to confirm or contradict the current finding of a relation in the behavior of THR and CHR. Moreover, for understanding of energy balance of MLT region, it is desirable produce similar analysis on global scales with annual variations. Nevertheless, we may expect similar behavior for global scales. The vertical turbulent diffusion coefficient is proportional to the first power of THR (Weinstock 1978). From the other hand, atomic oxygen fluxes from region of atomic oxygen production (above 110 km), and, consequently, atomic oxygen concentrations, are proportional to the vertical turbulent diffusion coefficient (e.g., Swenson et al. 2021; and references therein). In turn, CHR are quadratically proportional to the atomic oxygen concentration (Eq. 6). Hence, in absence of strong upward advective fluxes, which may reduce turbulent flux of atomic oxygen, the CHR will grow with rising of THR.

5 Summary and conclusions

For the first time we derived CHR from exothermic chemical reactions and THR based on common volume rocket experiment. We found that the second are smaller through the entire mesopause for nighttime conditions, except for a few THR peaks with width of several hundred meters. We also confirm the finding of other authors that approximately above 95 km the most essential contribution to the CHR comes from the recombination reaction of atomic oxygen, while below the reaction of atomic hydrogen with ozone is the leading one. Our derivation was based on assumption about photochemical ozone equilibrium. We proved this assumption and found that the ozone was in photochemical equilibrium in time of rocket flight above eighty kilometers. The

method for calculations of total CHR applied in the paper could be useful for future rocket borne and satellite missions if measured atomic oxygen concentrations and any second component of odd-oxygen—odd-hydrogen chemistry in mesopause region.

Additionally, we show an approach for calculation of efficiency for one of the most important exothermic reaction of ozone with atomic hydrogen if the temperature and atomic oxygen concentrations are known.

Appendix A

Here we consider the chemical heat for day and nighttime conditions ultimately from exothermic chemical reactions (1–7 in Table 1). The processes of radiative excitation by sunlight followed by relaxation and thermalization are excluded from this consideration.

In the 80–100 km region, the photochemical lifetime of atomic oxygen exceeds one day, thus day/night variations in atomic oxygen concentration are determined by dynamic processes (Allen et al. 1984; Shimazaki 1984; Brasseur and Solomon 2005; Strelnikov et al. 2019). Let's consider the case when day and night fluxes of atomic oxygen are approximately equal and thus $O_{day} \approx O_{night} \equiv O$.

The ozone balance equation for the daytime conditions is:

$$r_2 M \cdot O \cdot O_2 = r_4 H^d \cdot O_3^d + r_3 O \cdot O_3^d + J \cdot O_3^d, \quad \text{(A1)}$$

where J means ozone dissociation rates, superscript d denotes daytime values, and all other designations as in the main text of the article. Here for completeness we have retained the term with the reaction of atomic oxygen and ozone. In addition, in contrast to the more traditional balance equation, which considers only dissociation as the main process of ozone destruction, we have added the reaction of ozone with atomic hydrogen, since it was shown to be essential in the daytime balance equation (Kulikov et al. 2017, 2022a, b).

Let us write down the equation for chemical heat during daytime. Since we have seen that the reaction of ozone with atomic oxygen can be the second most important in some region, let us add it to the formula for the main part of chemical energy release as well:

$$E^d = \epsilon_1 r_1 M \cdot O^2 + \epsilon_2 r_2 M \cdot O \cdot O_2 + \varepsilon \cdot \epsilon_4 r_4 H^d \cdot O_3^d + \epsilon_3 r_3 O \cdot O_3^d. \quad \text{(A2)}$$

Substituting into the third term of (A2) product $r_4 H^d \cdot O_3^d$ from the ozone balance equation and reorganizing the terms we obtain:

$$\begin{aligned} E^d =& \epsilon_1 r_1 M \cdot O^2 + (\epsilon_2 + \varepsilon \cdot \epsilon_4) r_2 M \cdot O \cdot O_2 \\ &+ (\epsilon_3 - \varepsilon \cdot \epsilon_4) r_3 O \cdot O_3^d - \varepsilon \cdot \epsilon_4 J \cdot O_3^d. \end{aligned} \quad \text{(A3)}$$

The extended, as above, ozone balance equation and equation for chemical energy release at nighttime conditions can be written as follows:

$$r_2 M \cdot O \cdot O_2 = r_4 H^n \cdot O_3^n + r_3 O \cdot O_3^n, \quad \text{(A4)}$$

$$E^n = \epsilon_1 r_1 M \cdot O^2 + \epsilon_2 r_2 M \cdot O \cdot O_2 + \varepsilon \cdot \epsilon_4 r_4 H^n \cdot O_3^n + \epsilon_3 r_3 O \cdot O_3^n. \quad \text{(A5)}$$

Substituting first term from right-hand-side of (A4) into the third term of (A5) we get:

$$E^n = \epsilon_1 r_1 M \cdot O^2 + (\epsilon_2 + \varepsilon \cdot \epsilon_4) r_2 M \cdot O \cdot O_2 + (\epsilon_3 - \varepsilon \cdot \epsilon_4) r_3 O \cdot O_3^n. \quad \text{(A6)}$$

Comparing (A3) and (A6) one can see that the first and second terms are the same for both. The difference $\epsilon_3 - \varepsilon \cdot \epsilon_4$ is positive because $\epsilon_3 > \epsilon_4$ and $\varepsilon < 1$, hence second term is positive. Nighttime ozone concentrations at 80 km and above is larger than those in the daytime, $O_3^n > O_3^d$ (Allen et al. 1984; Sonnemann et al. 2007; Hartogh et al. 2011; Smith et al. 2013), hence, the third term of (A6) is larger than in (A3). The last negative term is present only in (A3), consequently, if downward fluxes of atomic oxygen for the daytime is equal to or smaller than those in night, or upward fluxes for the daytime is larger or equal to those for the daytime, inequality $E^n > E^d$ will be fulfilled.

Abbreviations

SABER	Sounding of the Atmosphere using Broadband Emission Radiometry
TIMED	Thermosphere Ionosphere Mesosphere Energetics and Dynamics
MLT	Mesosphere–lower thermosphere
R	Reaction
GWs	Gravity waves
CHR	Chemical heating rates
THR	Turbulent heating rates
WADIS	Wave propagation and dissipation in the middle atmosphere
CONE	Combined sensor for neutrals and electrons
FIPEX	Flux probe experiment
IAP	Leibniz-Institute of Atmospheric Physics at the University of Rostock
3D	Three dimensional
MIL	Mesosphere inversion layer
SME	Solar mesosphere explorer
LIDAR	Light detection and ranging
IRS	Institute of Space Systems at the University of Stuttgart
NRLMSISE	Naval Research Laboratory Mass Spectrometer Incoherent Scatter Radar Extended
LHS	Left-hand-side
SMILES/ISS	Submillimeter-Wave Limb-Emission Sounder/International Space Station
UTC	Coordinated universal time

Acknowledgements
The authors thank DLR-MORABA for their excellent contribution to the project by developing the complicated WADIS payload and campaign support together with the Andøya Space Center, as well as H.-J. Heckl for building the rocket instrumentation. We are grateful to Prof. Dr. A. Kutepov for helpful discussions and a reference to work of Khomich et al. (2008). The authors are grateful SABER team for data availability. We are thankful to editor Hidekatsu Jin for help in evaluating this paper and to two anonymous referees for their useful comments and improvements to the paper.

Author contributions
MG, BS, IS, MR, FJL, CSch, CSt, ME, SL, and SF worked on the calculations, visualization, analyzed and interpreted the data. All authors read and approved the final manuscript.

Funding
The work was supported by the German Space Agency (DLR) under grant 50OE1001 (project WADIS).

Availability of data and materials
The results of measurements and calculations are stored at https://www.radar-service.eu/radar/en/dataset/m2d4saqpb67y7dh5?token=mjLBEwnOVUtuzhFyyAWi.

Declarations

Ethics approval and consent to participate
Not applicable.

Competing interests
The authors declare that they have no conflict of interest.

Author details
[1]Leibniz-Institute of Atmospheric Physics at the University of Rostock, Schloss-Str. 6, 18225 Ostseebad Kühlungsborn, Germany. [2]German Aerospace Center, Institut of Atmospheric Physics, Oberpfaffenhofen, Germany. [3]University of Stuttgart, Institute of Space Systems, Stuttgart, Germany.

Received: 13 September 2024 Accepted: 18 December 2024
Published online: 30 December 2024

References

Adler-Golden S (1997) Kinetic parameters for OH nightglow modeling consistent with recent laboratory measurements. J Geophys Res 102(A9):19969–19976. https://doi.org/10.1029/97JA01622

Allen M, Lunine JI, Yung YL (1984) The vertical distribution of ozone in the mesosphere and lower thermosphere. J Geophys Res 89:4841–4872. https://doi.org/10.1029/JD089iD03p04841

Baron P, Dupuy E, Urban J, Murtagh DP, Eriksson P, Kasai Y (2009) HO_2 measurements in the stratosphere and the mesosphere from the sub-millimetre limb sounder Odin/SMR. Int J Remote Sens 30(15–16):4195–4208. https://doi.org/10.1080/01431160902822831

Bevington PR, Robinson DK (2003) Data reduction and error analysis for the physical sciences. 3rd edn, McGraw-Hill Companies Inc., New York. ISBN 0-07-247227-8

Brasseur G, Offermann D (1986) Recombination of atomic oxygen near the mesopause: interpretation of rocket data. J Geophys Res 91(D10):10818–10824. https://doi.org/10.1029/JD091iD10p10818

Brasseur G, Solomon S (2005) Aeronomy of the middle atmosphere–chemistry and physics of the stratosphere and mesosphere, 3rd edn. Atmospheric and Oceanographic Sciences Library 32, Springer, Dordrecht. ISBN 978-1-4020-3284-4. https://doi.org/10.1007/1-4020-3824-0

Burkholder JB, Sander SP, Abbatt J, Barker JR, Cappa C, Crounse JD, Dibble TS, Huie RE, Kolb CE, Kurylo MJ, Orkin VL, Percival CJ, Wilmouth DM, Wine PH (2020) Chemical kinetics and photochemical data for use in atmospheric studies. Evaluation No. 19, JPL Publication 19-5, Jet Propulsion Laboratory, Pasadena. http://jpldataeval.jpl.nasa.gov

Campbell IM, Gray CN (1973) Rate constants for $O(^3P)$ recombination and association with $N(^4S)$. Chem Phys Lett 18(4):607–609. https://doi.org/10.1016/0009-2614(73)80479-8

Caridade PJSB, Horta JZJ, Varandas AJC (2013) Implications of the O + OH reaction in hydroxyl nightglow modeling. Atmos Chem Phys 13:1–13. https://doi.org/10.5194/acp-13-1-2013

Chandra S (1980) Energetics and thermal structures of the middle atmosphere. Planet Space Sci 28:585–593. https://doi.org/10.1016/0032-0633(80)90004-5

Crutzen PJ (1971) Energy conversions and mean vertical motions in the high latitude summer mesosphere and lower thermosphere. In: Fiocco G, Reidel D (eds) Mesospheric Models and Related Experiments, pp 78–88. Springer, Dordrecht

Eberhart M, Löhle S, Steinbeck A, Binder T, Fasoulas S (2015) Measurement of atomic oxygen in the middle atmosphere using solid electrolyte sensors and catalytic probes. Atmos Meas Tech 8:3701–3714. https://doi.org/10.5194/amt-8-3701-2015

Eberhart M, Löhle S, Strelnikov B, Hedin J, Khaplanov M, Fasoulas S, Gumbel J, Lübken FJ, Rapp M (2019) Atomic oxygen number densities in the MLT region measured by solid electrolyte sensors on WADIS-2. Atmos Meas Tech 12:2445–2461. https://doi.org/10.5194/amt-12-2445-2019

Esplin R, Mlynczak MG, Russell J, Gordley L (2023) Sounding of the atmosphere using broadband emission radiometry (SABER): instrument and science measurement description. Earth Space Sci 10:e2023EA002999. https://doi.org/10.1029/2023EA002999

Fytterer T, von Savigny C, Mlynczak M, Sinnhuber M (2019) Model results of OH airglow considering four different wavelength regions to derive night-time atomic oxygen and atomic hydrogen in the mesopause region. Atmos Chem Phys 19:1835–1851. https://doi.org/10.5194/acp-19-1835-2019

Garcia RR, Solomon S (1983) A numerical model of the zonally averaged dynamical and chemical structure of the middle atmosphere. J Geophys Res 88(C2):1379–1400. https://doi.org/10.1029/JC088iC02p01379

Garcia RR, Solomon S (1985) The effect of breaking gravity waves on the dynamics and chemical composition of the mesosphere and lower thermosphere. J Geophys Res 90:3850–3868. https://doi.org/10.1029/JD090iD02p03850

Gordiets BF, Kulikov YN, Markov MN, Marov MY (1982) Numerical modeling of the thermospheric heat budget. J Geophys Res 87(A6):4504–4514. https://doi.org/10.1029/JA087iA06p04504

Grygalashvyly M, Becker E, Sonnemann GR (2011) Wave mixing effects on minor chemical constituents in the MLT region: results from a global CTM driven by high-resolution dynamics. J Geophys Res 116:D18302. https://doi.org/10.1029/2010JD015518

Grygalashvyly M, Becker E, Sonnemann GR (2012) Gravity wave mixing and effective diffusivity for minor chemical constituents in the mesosphere/lower thermosphere. Space Sci Rev 168:333–362. https://doi.org/10.1007/s11214-011-9857-x

Grygalashvyly M, Eberhart M, Hedin J, Strelnikov B, Lübken FJ, Rapp M, Löhle S, Fasoulas S, Khaplanov M, Gumbel J, Vorobeva E (2019) Atmospheric band fitting coefficients derived from a self-consistent rocket-borne experiment. Atmos Chem Phys 19:1207–1220. https://doi.org/10.5194/acp-19-1207-2019

Grygalashvyly M, Pogoreltsev AI, Andreyev AB, Smyshlyaev SP, Sonnemann GR (2021) Semi-annual variation of excited hydroxyl emission at mid-latitudes. Ann Geophys 39:255–265. https://doi.org/10.5194/angeo-39-255-2021

Hartogh P, Jarchow CH, Sonnemann GR, Grygalashvyly M (2011) Ozone distribution in the middle latitude mesosphere as derived from microwave measurements at Lindau (51.66°N, 10.13°E). J Geophys Res 116:D04305. https://doi.org/10.1029/2010JD014393

Hauchecorne A, Chanin ML, Wilson R (1987) Mesospheric temperature inversion and gravity wave dynamics. Geophys Res Lett 14:935–939. https://doi.org/10.1029/GL014i009p00933

Hickey MP, Walterscheid RL (1994) Wave-modified mean exothermic heating in the mesopause region. Geophys Res Lett 21(22):2413–2416. https://doi.org/10.1029/94GL02504

Hickey MP, Huang TY, Walterscheid RL (2003) Gravity wave packet effects on chemical exothermic heating in the mesopause region. J Geophys Res 108:1448–1454. https://doi.org/10.1029/2002JA009363

Hocking WK (1990) Turbulence in the region 80–120 km. Adv Space Res 10(12):153–161. https://doi.org/10.1016/0273-1177(90)90394-F
Hunt BG (1972) Photochemical heating of the mesosphere and lower thermosphere. Tellus 24(1):47–55. https://doi.org/10.3402/tellusa.v24i1.10619
Justus CG (1967) The eddy diffusivities, energy balance parameters and heating rates of upper atmospheric turbulence. J Geophys Res 72:1035–1039. https://doi.org/10.1029/JZ072i003p01035
Kalogerakis KS (2019) A previously unrecognized source of the O_2 atmospheric band emission in Earth's nightglow. Sci Adv 5:eaau9255. https://doi.org/10.1126/sciadv.aau9255
Kalogerakis KS, Matsiev D, Sharma RD, Wintersteiner PP (2016) Resolving the mesospheric nighttime 4.3 μm emission puzzle: laboratory demonstration of new mechanism for OH(υ) relaxation. Geophys Res Lett 43:8835–8843. https://doi.org/10.1002/2016GL069645
Kellogg WW (1961) Chemical heating above the polar mesopause in winter. J Atmos Sci 18(3):373–381. https://doi.org/10.1175/1520-0469(1961)018%3c0373:CHATPM%3e2.0.CO;2
Khomich VYu, Semenov AI, Shefov NN (2008) Airglow as an indicator of upper atmospheric structure and dynamics. Springer-Verlag, Berlin, Heidelberg. https://doi.org/10.1007/978-3-540-75833-4
Kreyling D, Sagawa H, Wohltmann I, Lehmann R, Kasai Y (2013) SMILES zonal and diurnal variation climatology of stratospheric and mesospheric trace gasses: O_3, HCl, HNO_3, ClO, BrO, HOCl, HO_2, and temperature. J Geophys Res Atmos 118:11888–11903. https://doi.org/10.1002/2012JD019420
Kulikov MY, Belikovich MV, Grygalashvyly M, Sonnemann GR, Ermakova TS, Nechaev AA, Feigin AM (2017) Daytime ozone loss term in the mesopause region. Ann Geophys 35:677–682. https://doi.org/10.5194/angeo-35-677-2017
Kulikov MY, Belikovich MV, Grygalashvyly M, Sonnemann GR, Ermakova TS, Nechaev AA, Feigin AM (2018) Nighttime ozone chemical equilibrium in the mesopause region. J Geophys Res 123:3228–3242. https://doi.org/10.1002/2017JD026717
Kulikov MY, Nechaev AA, Belikovich MV, Vorobeva EV, Grygalashvyly M, Sonnemann GR, Feigin AM (2019) Boundary of nighttime ozone chemical equilibrium in the mesopause region from SABER data: implications for derivation of atomic oxygen and atomic hydrogen. Gepohys Res Lett 46:997–1004. https://doi.org/10.1029/2018GL080364
Kulikov MY, Belikovich MV, Feigin AM (2021) The 2-day photochemical oscillations in the mesopause region: the first experimental evidence? Geophys Res Lett 48:e092795. https://doi.org/10.1029/2021GL092795
Kulikov MY, Belikovich MV, Grygalashvyly M, Sonnemann GR, Feigin AM (2022a) Retrieving daytime distributions of O, H, OH, HO_2, and chemical heating rate in the mesopause region from satellite observations of ozone and OH* volume emission: the evaluation of the importance of the reaction $H+O_3 \rightarrow O_2+OH$ in the ozone balance. Adv Space Res 69(9):3362–3373. https://doi.org/10.1016/j.asr.2022.02.011
Kulikov MY, Belikovich MV, Grygalashvyly M, Sonnemann GR, Feigin AM (2022b) The revised method for retrieving daytime distributions of atomic oxygen and odd-hydrogens in the mesopause region from satellite observations. Earth Planets Space 74:44. https://doi.org/10.1186/s40623-022-01603-580-8
Kulikov MY, Belikovich MV, Chubarov AG, Dementeyva SO, Feigin AM (2023) Boundary of nighttime ozone chemical equilibrium in the mesopause region: improved criterion of determining the boundary from satellite data. Adv Space Res 71(6):2770–2780. https://doi.org/10.1016/j.asr.2022.11.005
Kulikov MY, Belikovich MV, Chubarov AG, Dementyeva SO, Feigin AM (2024) Technical note: nighttime OH and HO_2 chemical equilibria in the mesosphere – lower thermosphere. Atmos Chem Phys 24(18):10965–10983. https://doi.org/10.5194/acp-24-10965-2024
Lübken FJ (1997) Seasonal variation of turbulent energy dissipation rates at high latitudes as determined by in situ measurements of neutral density fluctuations. J Geophys Res 102(D12):13441–13456. https://doi.org/10.1029/97JD00853
Lübken FJ, Hillert W, Lehmacher G, von Zahn U (1993) Experiments revealing small impact of turbulence on the energy budget of the mesosphere and lower thermosphere. J Geophys Res 98(D11):20369–20384. https://doi.org/10.1029/93JD02055
Lübken FJ, Rapp M, Hoffmann P (2002) Neutral air turbulence and temperatures in the vicinity of polar mesosphere summer echoes. J Geophys Res 107(D15):4273–4277. https://doi.org/10.1029/2001JD000915
Makhlouf UB, Picard RH, Winick JR (1995) Photochemical-dynamical modeling of the measured response of airglow to gravity waves. J Geophys Res 100(D6):11289–11311. https://doi.org/10.1029/94JD03327
McDade IC, Llewellyn EJ (1991) Comment on "middle atmosphere heating by exothermic chemical reactions involving odd-hydrogen species." Geophys Res Lett 18:1791–1792. https://doi.org/10.1029/91GL02138
McDade IC, Llewellyn EJ (1993) An assessment of the $H+O_3$ heating efficiencies in the nighttime mesopause region. Ann Geophys 11:47–51
Meriwether JW, Mlynczak MG (1995) Is chemical heating a major cause of the mesosphere inversion layer? J Geophys Res 100(D1):1379–1387. https://doi.org/10.1029/94JD01736
Millàn L, Wang S, Livesey N, Kinnison D, Sagawa H, Kasai Y (2015) Stratospheric and mesospheric HO_2 observations from the Aura Microwave Limb Sounder. Atmos Chem Phys 15:2889–2902. https://doi.org/10.5194/acp-15-2889-2015
Minschwaner K, Manney GL, Wang S, Harwood RS (2011) Hydroxyl in the stratosphere and mesosphere – part 1: diurnal variability. Atmos Chem Phys 11:955–962. https://doi.org/10.5194/acp-11-955-2011
Minzner RA (1977) The 1976 Standard Atmosphere and its relationship to earlier standards. Rev Geophys 15:375–384. https://doi.org/10.1029/RG015i003p00375
Mlynczak MG (1997) Energetics of the mesosphere and lower thermosphere and the SABER experiment. Adv Space Res 20(6):1177–1183. https://doi.org/10.1016/S0273-1177(97)00769-2
Mlynczak MG, Solomon S (1991) Middle atmosphere heating by exothermic chemical reactions involving odd-hydrogen species. Geophys Res Lett 18(1):37–40. https://doi.org/10.1029/90GL02672
Mlynczak MG, Solomon S (1993) A detailed evaluation of the heating efficiency in the middle atmosphere. J Geophys Res 98(D6):10517–10541. https://doi.org/10.1029/93JD00315
Mlynczak MG, Marshall BT, Martin-Torres FJ, Russell JM III, Thompson RE, Remsberg EE, Gordley LL (2007) Sounding of the Atmosphere using Broadband Emission Radiometry observations of daytime mesospheric O2(1Δ) 1.27 μm emission and derivation of ozone, atomic oxygen, and solar and chemical energy deposition rates. J Geophys Res 112:D15306. https://doi.org/10.1029/2006JD008355
Mlynczak MG, Hunt LA, Mast JC, Marshall BT, Russell JM III, Smith AK, Siskind DE, Yee JH, Mertens CJ, Martin-Torres FJ, Thompson RE, Drob DP, Gordley LL (2013a) Atomic oxygen in the mesosphere and lower thermosphere derived from SABER: algorithm theoretical basis and measurement uncertainty. J Geophys Res 118:5724–5735. https://doi.org/10.1002/jgrd.50401
Mlynczak MG, Hunt LA, Mertens CJ, Marshall BT, Russell JM III, Lòpez-Puertas M, Smith AK, Siskind DE, Mast JC, Thompson RE, Gordley LL (2013b) Radiative and energetic constraints on the global annual mean atomic oxygen concentration in the mesopause region. J Geophys Res Atmos 118:5796–5802. https://doi.org/10.1002/jgrd.50400
Mlynczak MG, Hunt LA, Marshall BT, Mertens CJ, Russell JM III, Siskind DE, Thompson RE, Gordley LL (2013c) Radiative constraints on the minimum atomic oxygen concentration in the mesopause region. Geophys Res Lett 40:3777–3780. https://doi.org/10.1002/grl.50725
Mlynczak MG, Hunt LA, Marshall BT, Mertens CJ, Marsh DR, Smith AK, Russell JM, Siskind DE, Gordley LL (2014) Atomic hydrogen in the mesopause region derived from SABER: algorithm theoretical basis, measurement uncertainty, and results. J Geophys Res Atmos 119:3516–3526. https://doi.org/10.1002/2013JD021263
Mlynczak MG, Hunt LA, Russell JM III, Marshall BT (2018) Updated SABER night atomic oxygen and implications for SABER ozone and atomic hydrogen. Geophys Res Lett 45:5735–5741. https://doi.org/10.1029/2018GL077377
Picone JM, Hedin AE, Drob DP, Aikin AC (2002) NRLMSISE-00 empirical model of the atmosphere: statistical comparisons and scientific issues. J Geophys Res 107(A12):1468. https://doi.org/10.1029/2002JA009430
Ramesh K, Sridharan S, Rao SVB (2013) Dominance of chemical heating over dynamics in causing a few large mesospheric inversion layer events during January-February 2011. J Geophys Res 118:6751–6765. https://doi.org/10.1002/jgra.50601

Ramesh K, Sridharan S, Rao SVB (2014) Causative mechanisms for the occurrence of a triple layered mesospheric inversion event over low latitudes. J Geophys Res 119:3930–3943. https://doi.org/10.1002/2013JA019750
Ramesh K, Sridharan S, Rao SVB (2015) Influence of solar cycle and chemistry on tropical (10°N–15°N) mesopause variabilities. J Geophys Res 120:4038–4051. https://doi.org/10.1002/2014JA020930
Ramesh K, Sridharan S, Raghunath K, Rao SVB (2017) A chemical perspective of day and night tropical (10°N–15°N) mesospheric inversion layers. J Geophys Res 122:3650–3664. https://doi.org/10.1002/2016JA023721
Riese M, Offermann D, Brasseur G (1994a) Energy released by recombination of atomic oxygen and related species at mesopause heights. J Gepohys Res 99:14585–14594. https://doi.org/10.1029/94JD00356
Riese M, Offermann D, Brasseur G (1994b) Recombination energy of atomic oxygen and related species at the mesopause. Adv Space Res 14(9):177–180. https://doi.org/10.1016/0273-1177(94)90132-5
Schmidlin FJ (1976) Temperature inversions near 75 km. Geophys Res Lett 3(3):173–176. https://doi.org/10.1029/GL003i003p00173
Sharma RD, Wintersteiner PP, Kalogerakis KS (2015) A new mechanism for OH vibrational relaxation leading to enhanced CO_2 emissions in the nocturnal atmosphere. Geophys Res Lett 42:4639–4647. https://doi.org/10.1002/2015GL063724
She CY, Yu JR, Chen H (1993) Observed thermal structure of a midlatitude mesopause. Geophys Res Lett 20:567–570. https://doi.org/10.1029/93gl00808
Shimazaki T (1984) The photochemical time constants of minor constituents and their families in the middle atmosphere. J Atmos Terr Phys 46(2):173–191. https://doi.org/10.1016/0021-9169(84)90143-0
Smith AK, Marsh DR, Szymczak AC (2003) Interaction of chemical heating and the diurnal tide in the mesosphere. J Geophys Res 108(D5):4164. https://doi.org/10.1029/2002JD002664
Smith AK, Marsh DR, Russell JM III, Mlynczak MG, Martin-Torres FJ, Kyrölä E (2008) Satellite observations of high nighttime ozone at the equatorial mesopause. J Geophys Res 113:D17312. https://doi.org/10.1029/2008JD010066
Smith AK, Harvey VL, Mlynczak MG, Funke B, Garcia-Comas M, Hervig M, Kaufmann M, Kyrölä E, López-Puertas M, McDade I, Randall CE, Russell JM III, Sheese PE, Shiotani M, Skinner WR, Suzuki M, Walker KA (2013) Satellite observations of ozone in the upper mesosphere. J Geophys Res Atmos 118:5803–5821. https://doi.org/10.1002/jgrd.50445
Smith AK, López-Puertas M, Xu J, Mlynczak MG (2015) The heating efficiency of the exothermic reaction $H + O_3$ in the mesosphere. J Geophys Res Atmos 120:12739–12747. https://doi.org/10.1002/2015JD024061
Sonnemann GR, Grygalashvyly M (2020) The slow-down effect in the nighttime mesospheric chemistry of hydrogen radicals. Adv Space Res 65(12):2800–2807. https://doi.org/10.1016/j.asr.2020.03.025
Sonnemann G, Kremp Ch, Ebel A, Berger U (1997) Calculation of the global chemical heating rates by means of a 3d-model of dynamics and chemistry. Adv Space Res 20(6):1153–1156. https://doi.org/10.1016/S0273-1177(97)00762-X
Sonnemann G, Kremp Ch, Ebel A, Berger U (1998) A three-dimensional dynamic model of the minor constituents of the mesosphere. Atmos Environ 32:3157–3172. https://doi.org/10.1016/S1352-2310(98)00113-7
Sonnemann GR, Hartogh P, Jarchow C, Grygalashvyly M, Berger U (2007) On the winter anomaly of the night-to-day ratio of ozone in the middle to upper mesosphere in middle to high latitudes. Adv Space Res 40:846–854. https://doi.org/10.1016/j.asr.2007.01.039
Strelnikov B, Szewczyk A, Strelnikova I, Latteck R, Baumgarten G, Lübken FJ, Rapp M, Fasoulas S, Löhle S, Eberhart M, Hoppe UP, Dunker T, Friedrich M, Hedin J, Khaplanov M, Gumbel J, Barjatya A (2017) Spatial and temporal variability in MLT turbulence inferred from in situ and ground based observations during the WADIS-1 sounding rocket campaign. Ann Geophys 35:547–565. https://doi.org/10.5194/angeo-35-547-2017
Strelnikov B, Staszak T, Strelnikova I, Lübken FJ, Grygalashvyly M, Hedin J, Khaplanov M, Gumbel J, Fasoulas S, Löhle S, Eberhart M, Baumgarten G, Höffner J, Wörl R, Rapp M, Friedrich M (2019) Simultaneous in situ measurements of small-scale structures in neutral, plasma, and atomic oxygen densities during WADIS sounding rocket project. Atmos Chem Phys 19:11443–11460. https://doi.org/10.5194/acp-19-11443-2019
Strelnikov B, Rapp M, Fritts DC, Wang L (2023) Assessment of the precision of spectral model turbulence analysis techniques using direct numerical simulation data. J Geophys Res 127(4):e2021JD035516. https://doi.org/10.1029/2021JD035516
Strelnikov B, Rapp M, Lübken FJ (2013) In-situ density measurements in the mesosphere/lower thermosphere region with the TOTAL and CONE instruments. In: Oyama K (ed) An introduction to space instrumentation. Terra Publishers. https://doi.org/10.5047/isi.2012.001
Sutherland W (1893) LII. The viscosity of gases and molecular force. London Edinburgh Dublin Philos Mag J Sci 36(223):507–531. https://doi.org/10.1080/14786449308620508
Swenson GR, Vargas F, Jones M, Zhu Y, Kaufmann M, Yee JH, Mlynczak M (2021) Intra-annual variation of eddy diffusion (k_{zz}) in the MLT, from SABER and SCIAMACHY atomic oxygen climatologies. J Geophys Res 126:e2021JD035343. https://doi.org/10.1029/2021JD035343
Szewczyk A, Strelnikov B, Rapp M, Strelnikova I, Baumgarten G, Kaifler N, Dunker T, Hoppe UP (2013) Simultaneous observations of a mesospheric inversion layer and turbulence during the ECOMA-2010 rocket campaign. Ann Geophys 31:775–785. https://doi.org/10.5194/angeo-31-775-2013
Tatarskii VI (1971) The effects of the turbulent atmosphere on wave propagation. Israel Program for Scientific Translations, Jerusalem
von Zahn U, Lübken FJ, Pütz C (1990) BUGATTI experiments: mass spectrometric studies of lower thermosphere eddy mixing and turbulence. J Geophys Res 95(D6):7443–7465. https://doi.org/10.1029/jd095id06p07443
Wang S, Zhang Q, Millàn L, Li KF, Yung YL, Sander SP, Livesey NJ, Santee ML (2015) First evidence of middle atmospheric HO_2 response to 27 day solar cycles from satellite observations. Geophys Res Lett 42:10004–10009. https://doi.org/10.1002/2015GL065237
Ward WE, Fomichev VI (1993) On the role of atomic oxygen in the dynamics and energy budget of the mesosphere and lower thermosphere. Geophys Res Lett 20(12):1199–1202. https://doi.org/10.1029/93GL00842
Ward WE, Fomichev VI (1996) Consequences of CO_2-O collisional relaxation on the energy budget of the mesosphere and lower thermosphere. Adv Space Res 17(11):127–137. https://doi.org/10.1016/0273-1177(95)00740-6
Weinstock J (1978) Vertical turbulent diffusion in a stably stratified fluid. J Atmos Sci 35:1022–1027. https://doi.org/10.1175/1520-0469(1978)035%3c1022:VTDIAS%3e2.0.CO;2
Xu J, Wang Y, Wang Y (2000) The loss of photochemical heating caused by gravity waves in the mesopause region. J Atmos Sol Terr Phys 62(1):37–45. https://doi.org/10.1016/S1364-6826(99)00091-7
Xu J, Gao H, Smith AK, Zhu Y (2012) Using TIMED/SABER nightglow observations to investigate hydroxyl emission mechanisms in the mesopause region. J Geophys Res 117:D02301. https://doi.org/10.1029/2011JD016342
Zhu Y, Kaufmann M (2019) Consistent nighttime atomic oxygen concentrations from O_2 A-band, O(^{1}S) green line, and OH airglow measurements as performed by SCIAMACHY. Geophys Res Lett 46:8536–8545. https://doi.org/10.1029/2019GL083550

Publisher's Note